MCDHF calculations of the electric dipole moment of radium induced by the nuclear Schiff moment

Jacek Bieroń
Instytut Fizyki imienia Mariana Smoluchowskiego, Uniwersytet Jagielloński Reymonta 4, 30-059 Kraków, Poland

Gediminas Gaigalas and Erikas Gaidamauskas
Vilnius University Research Institute of Theoretical Physics and Astronomy, A. Goštauto 12, LT-01108 Vilnius, Lithuania and Vilnius Pedagogical University, Studentų 39, LT-08106 Vilnius, Lithuania

Stephan Fritzsche
Helmholtzzentrum für Schwerionenforschung (GSI), D-64291 Darmstadt, Germany

Paul Indelicato
Laboratoire Kastler Brossel, École Normale Supérieure CNRS; Université P. et M. Curie - Paris 6 Case 74; 4, place Jussieu, 75252 Paris CEDEX 05, France

Per Jönsson
Nature, Environment, Society Malmö University, S-205 06 Malmö, Sweden

(Dated: April 6, 2009)

The multiconfiguration Dirac-Hartree-Fock theory (MCDHF) has been employed to calculate the electric dipole moment of the $7s6d\ ^3D_2$ state of radium induced by the nuclear Schiff moment. The results are dominated by valence and core-valence electron correlation effects. We show that the correlation effects can be evaluated in a converged series of multiconfiguration expansions.

PACS numbers: 11.30.Er,21.10.Ky,24.80.+y,31.30.jg

I. INTRODUCTION

A non-zero permanent electric dipole moment (EDM) of an atom, molecule, or any other composite or elementary particle is one of the possible manifestations of parity (P) and time reversal (T) symmetry violations. In the absence of any external electromagnetic field an atom can have a permanent EDM either due to an intrinsic EDM of one of its constituent particles or due to P- and T-violating (P-odd and T-odd) interactions between these particles [1, 2]. When compared with the intrinsic EDM of the constituent particles, the net *induced* EDM of an atom or molecule is often expected to be larger by several orders of magnitude due to various nuclear and atomic enhancement mechanisms. Therefore, atoms and molecules are considered to be very attractive for carrying out EDM experiments and in the search for 'new physics' beyond the standard model, since, in the latter case, the induced EDM is greatly suppressed, when compared to the anticipated values from the 'new' theories [3]. In atomic physics, in particular, the experimental search for a permanent EDM is gaining momentum due to recent advancements in trapping free neutral atoms [4, 5, 6], including various radioactive species [7, 8].

During the last decade several atoms were considered as candidates for such experiments [3, 9]. These involved (i) diamagnetic atoms (i.e., total angular momentum $J = 0$) in their respective ground states, (ii) the alkalis, and (iii) atoms with a single p electron outside closed shells, which were investigated in laser traps for their prospectives to perform EDM experiments. Presently, radium appears to be the most promising candidate, and experiments on this element are under way at the Argonne National Laboratory [7, 10, 11] as well as the Kernfysisch Versneller Instituut [12, 13, 14]. The main advantages of radium lay in (i) large nuclear charge Z, (ii) simple electronic structure and closed-shell $[\mathrm{Kr}]4d^{10}4f^{14}5s^25p^65d^{10}6s^26p^67s^2\ ^1S_0$ ground state, (iii) octupole deformations of the radium nuclei for several isotopes [15, 16], as well as in (iv) coincidental proximity of two atomic levels of opposite parity, $7s7p\ ^3P_1$ and $7s6d\ ^3D_2$, which are separated by a very small energy interval 5.41 cm^{-1}. In particular, the latter two advantages give rise to a relatively large enhancement factor, which is one of the largest among the atoms considered so far [17, 18].

However, extraction of fundamental P- and T-violating parameters or coupling constants from experimentally

measured atomic EDM requires atomic form factors which can be provided only by an *ab initio* atomic theory. Several of these form factors have been previously calculated by the group of Flambaum [9, 17]. In practice, there are essentially four different form factors, related to four mechanisms which can induce an atomic EDM. An atom can acquire a permanent EDM due to P- and T-odd electron-nucleon interactions, or due to the electromagnetic interaction of atomic electrons with nuclear P- and T-odd moments, of which the leading ones are: the Schiff moment, the magnetic quadrupole moment, and the electric octupole moment, respectively. The latter two moments may exist only in nuclei with spins larger than $I = 1/2$, while the Schiff moment may exist also in isotopes with nuclear spin $I = 1/2$. Nuclei with spins larger than $I = 1/2$ produce electric quadrupole shifts which are difficult to account for in an EDM measurement. Therefore an EDM induced by the Schiff moment in $I = 1/2$ isotopes seems to be the property of choice among (most of) the experimenters [13, 19, 20]. The nuclear Schiff moment is a P-odd and T-odd (electric-dipole) moment that occurs due to P- and T-violating interactions at the nuclear scale. The Schiff moment mixes atomic states of opposite parity and may induce static EDM in atoms if magnetic and finite-size effects are taken into account in the electron-nucleus interaction [3].

In the present paper, we present calculations for the atomic EDM in radium, as induced by the Schiff moment. The atomic wave functions were obtained within the framework of the multiconfiguration Dirac-Hartree-Fock (MCDHF) theory. The wave functions were separately optimized for the $7s6d\ ^3D_2$ and $7s7p\ ^3P_1$ states (similar calculations were carried out recently for the scalar-pseudoscalar contribution to the EDM in cesium [21]). The main purpose of this paper is to provide a systematic evaluation of the effects of electron correlation on the calculated EDM of radium. We demonstrate the saturation of the core-valence correlations, the dominant electron correlation effect beyond the Dirac-Fock approximation.

II. THEORY

The Hartree-Fock and Dirac-Hartree-Fock theories, based either on the finite-grid, basis-set, or some other numerical methods provide a natural point of departure in describing the electronic structure of atoms and molecules. For medium and heavy elements, these methods are often combined with Breit-Pauli or Dirac-Coulomb-Breit Hamiltonians in order to account for relativistic and retardation effects on the wave functions and the level structure of complex atoms. However, the main hindrance in applying modern computational techniques arises from the electron-electron correlation, i.e., the residual interaction among the electrons beyond the atomic *mean* field, and this is especially true for systems with many electrons. In neutral or nearly-neutral systems, missing electron-correlation effects are indeed often the main reason for the discrepancies between the observed and calculated properties of atoms.

Today, many-body perturbation theory (MBPT) [22, 23, 24, 25] and various variational methods, often referred to as the multiconfiguration Hartree-Fock (MCHF) theory (or its relativistic counterpart — the Dirac-Hartree-Fock theory [26, 27, 28]) are the two dominant pillars in performing atomic structure calculations. These methods are designed to evaluate the electron correlation effects in a systematic manner. For MBPT and most related methods, a nearby closed-shell configuration of the atom or ion is typically a convenient starting point. During the past decades, therefore, MBPT techniques were mainly applied to systems with either no or just a single electron outside closed shells. Systems with several electrons in open shells are, in contrast, much more difficult to deal with if benefit is to be taken from the theory of angular momentum and spherical tensor operators, i.e., by using a *restricted* representation of the one-electron orbitals. Difficulties occur then due to the large departure from a closed-shell V^N potential and the rapid increase in the complexity of all perturbation expansions with any additional electron outside closed shells. Although in the variational multiconfiguration methods the algebraic complexity also depends on the shell structure of the atom, these methods can be applied more easily to systems with an arbitrary number of electrons outside closed shells. Apart from the number of open shells, the accuracy of multiconfiguration Dirac-Hartree-Fock calculations depends crucially also on the occupation of the valence shell(s) but this occurs rather indirectly, through the limiting number of configuration state functions that can be included in a particular wave function expansion. In this sense, the limitations are less conceptual but arise from the available computer resources. These limitations are typically related to the structure of the valence shell(s), i.e., to the angular properties of the valence electrons and their couplings.

A. MCDHF theory

We used a slightly modified version of the General Relativistic Atomic Structure Package (GRASP) [28] to generate the electronic wave functions. In the multiconfiguration Dirac-Hartree-Fock method, the wave function for a particular atomic state $\Psi(\gamma PJM_J)$ is obtained as a linear combination of configuration state functions (CSFs) which are eigenfunctions of the parity P and the total angular momentum operators J^2 and J_z,

$$\Psi(\gamma PJM_J) = \sum_r^{\mathrm{NCF}} c_r \Phi(\gamma_r PJM_J)\,. \qquad (1)$$

In the present computations, the wave functions were separately generated for the $7s7p\ ^3P_1$ and $7s6d\ ^3D_2$ states of radium. Each wave function was obtained as self-consistent solution of the Dirac-Hartree-Fock equa-

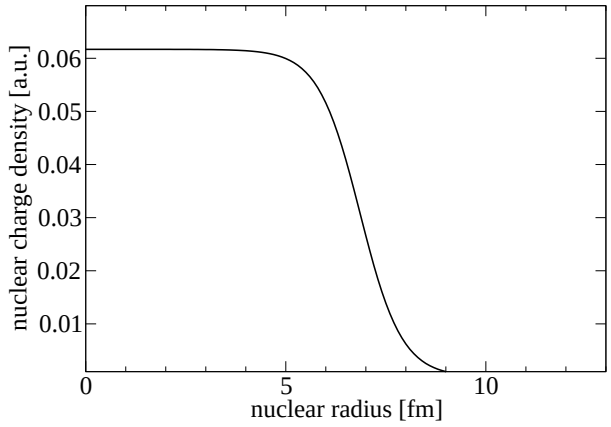

FIG. 1: Nuclear charge density ρ [a.u.] as function of the nuclear radius r [fm], using a two-parameter Fermi distribution for the $^{225}_{88}$Ra nucleus.

tions [26] by using a systematically increased multiconfiguration bases (of size NCF) of symmetry-adapted configuration state functions $\Phi(\gamma_r PJM_J)$. Configuration mixing coefficients c_r were obtained through the diagonalisation of the Dirac-Coulomb Hamiltonian

$$\hat{H}_{\rm DC} = \sum_{j=1}^{N} \left[c\boldsymbol{\alpha}_j \cdot \boldsymbol{p}_j + (\beta_j - 1)c^2 + V(r_j) \right] + \sum_{j>k} 1/r_{jk} \tag{2}$$

where $V(r)$ is the monopole part of the electron-nucleus interaction. A more detailed description of the theory [27, 29] and method of calculation [30, 31] can be found elsewhere.

B. Nuclear shape

All self-consistent-field calculations were done with the nucleus modelled as a spherical ball by applying a two-parameter Fermi distribution

$$\rho(r) = \frac{\rho_0}{1 + \exp[(r-c)/a]} \tag{3}$$

in order to approximate the radial dependence of the nuclear charge density $\rho(r)$. The parameter ρ_0 is derived from the normalization condition $\int \rho(r) d^3r = Ze$. Figure 1 shows the nuclear charge density $\rho(r)$ inside the $^{225}_{88}$Ra nucleus, calculated with the parameters $c =$ 6.85 fm and $a = 0.523$ fm (see [32, 33] for details). For the other two isotopes the 'half-charge-density' parameter c was set to $c = 6.83$ fm ($^{223}_{88}$Ra) and $c = 6.73$ fm ($^{213}_{88}$Ra), with the 'nuclear-skin-thickness' a value unchanged. These nuclear charge distributions were also used in the subsequent calculations of the Schiff moment expectation values (Eq. 14).

In the GRASP code [28] all electronic (radial) orbitals are represented on a numerical grid which increases exponentially in order to ensure an accurate representation of the atomic wave functions near the nucleus. The grid is generated from the formula $r_i = r_o \exp((i-1)h)$, with $r_o = 2.0 \times 10^{-8} \times a_0$, $h = 7.0 \times 10^{-3}$, and $i = 1, \ldots, 4000$. With the above parameters, there were 1255 grid points within the 'half-charge-density' nuclear radius $r_{\rm nuc} = 6.85$ fm, while the numerical representation of the full extent of all radial (core and valence) electronic orbitals required more than 3000 points. With the above choice of the radial grid, all necessary one- and two-particle matrix elements can be calculated with a (relative) accuracy of the order of $\sim 10^{-8}$ or better. Note however that larger uncertainties may arise from the radial matrix elements in Eq. (14), due to the approximate nature of the nuclear charge distribution in Eq. (3) and due to deviations from radial symmetry of those isotopes, for which nuclear deformations are significant (for model dependence see [34]).

C. Atomic EDM

Neglecting the contributions from the off-diagonal hyperfine interaction the coupled wave function of the total system 'electrons + nucleus' is given by the Clebsch-Gordan expansion [35]

$$\Psi\left(\gamma\nu PJIFM_F\right) = \sum_{M_J M_I} \langle JIM_J M_I | JIFM_F \rangle \; \Psi\left(\gamma PJM_J\right) \; \Psi\left(\nu IM_I\right) \tag{4}$$

where $\Psi\left(\nu IM_I\right)$ represents the ground state of the nucleus, and where the standard notation is used for the Clebsch-Gordan coefficients. For high-Z elements with closed levels of opposite parity, such as radium in the $^3P_1$ and $^3D_2$ levels, one of the most important parity (P) and time reversal symmetry (T) violating interactions is caused by the nuclear Schiff moment $\mathbf{S}$, which gives rise to the electron-nucleus interaction:

$$\hat{H}_{SM} = 4\pi \sum_{j=1}^{N} \left(\boldsymbol{S} \cdot \boldsymbol{\nabla}_j\right) \; \rho\left(r_j\right) . \tag{5}$$

In this Hamiltonian, $\rho\left(r\right)$ is the normalized to unity nuclear density function from Eq. (3), and the Schiff moment $\boldsymbol{S}$ is directed along the nuclear spin $\boldsymbol{I}$: $\boldsymbol{S} \equiv S\boldsymbol{I}/I$. The interaction in Eq. (5) mixes states of different parity and may also induce a static electric dipole moment of the atom. Since the Schiff moment interaction is quite weak, we can express the wave function of the (mixed-parity) hyperfine state $|F, M_F\rangle$ of the level J^P as [21]:

$$\widetilde{\Psi}\left(\gamma\nu JIFM_F\right) \;=\; a\Psi\left(\gamma\nu PJIFM_F\right) \,+\, \sum_{i=1}^{m} b_i\,\Psi\left(\alpha_i\nu(-P)J_iIFM_F\right) \tag{6}$$

where the coefficient a of the given hyperfine state can be set to 1. The expansion coefficients of the other (hyperfine) states of opposite parity can be perturbatively approximated by

$$b_i \;=\; \frac{\left\langle \Psi\left(\alpha_i\nu(-P)J_i\;IFM_F\right)|\hat{H}_{SM}|\Psi\left(\gamma\nu PJIFM_F\right)\right\rangle}{E\left(\gamma PJ\right) \;-\; E\left(\alpha_i(-P)J_i\right)}\,. \tag{7}$$

The mixed-parity wave function in Eq. (6) for the hyperfine state $|F, M_F\rangle$ of a particular atomic level $^{2S+1}L_J$ induces a static EDM of an atom:

$$D_A = \left\langle \widetilde{\Psi}\left(\gamma\nu JIFM_F\right)|\hat{D}_z|\widetilde{\Psi}\left(\gamma\nu JIFM_F\right)\right\rangle \;=\; 2\sum_{i=1}^{m} b_i \left\langle \Psi\left(\gamma\nu PJIFM_F\right)|\hat{D}_z|\Psi\left(\alpha_i\nu(-P)J_iIFM_F\right)\right\rangle \tag{8}$$

where $\hat{D}_z$ denotes the z projection of the electric-dipole moment operator. For this electric-dipole operator, the matrix element between (hyperfine) states of different parity can be expressed as:

$$\left\langle \Psi\left(\gamma\nu PJIFM_F\right)|\hat{D}_z|\Psi\left(\alpha_i\nu(-P)J_iIFM_F\right)\right\rangle \;=$$

$$(-1)^{I+J+F+1}\;(2F+1)\;\sqrt{2J+1}\;\begin{pmatrix} F & 1 & F \\ -M_F & 0 & M_F \end{pmatrix}\begin{Bmatrix} J & F & I \\ F & J_i & 1 \end{Bmatrix}\left[\Psi\left(\gamma PJ\right)\|\hat{D}^1\|\Psi\left(\alpha_i(-P)J_i\right)\right] \tag{9}$$

while the matrix element of the (scalar) electron-nucleus interaction in Eq. (5), induced by the Schiff moment, is written as:

$$\left\langle \Psi\left(\gamma\nu PJIFM_F\right)|\hat{H}_{SM}|\Psi\left(\alpha_i\nu(-P)J_i\;IFM_F\right)\right\rangle \;=$$

$$(-1)^{I+J+F+1}\;\sqrt{2J+1}\;\sqrt{\frac{(I+1)\,(2I+1)}{I}}\begin{Bmatrix} I & I & 1 \\ J_i & J & F \end{Bmatrix} 4\pi\; S\;\left[\Psi\left(\gamma PJ\right)\|\hat{\nabla}^1\,\rho\left(r\right)\|\Psi\left(\alpha_i(-P)J_i\right)\right] \tag{10}$$

and is independent of M_F. In the following, we shall refer to the last term on the right-hand side of Eq. (10) as the reduced matrix element of the Schiff operator for the two (fine-structure) levels J and J_i of different parity, and shall assume $M_F \;=\; F$, in line with optical pumping schemes of hyperfine levels with circularly polarized light. For the $|F, M_F\rangle$ hyperfine state of the $^3D_2$ level, the static EDM in Eq. (8), induced by the P-odd and T-odd nuclear Schiff moment, becomes

$$D_A(^3D_2,\,FM_F) \;=\; 2\,\frac{\left\langle \Psi\left(^3D_2,\,FM_F\right)|\hat{D}_z|\Psi\left(^3P_1,\,FM_F\right)\right\rangle\left\langle \Psi\left(^3P_1,\,FM_F\right)|\hat{H}_{SM}|\Psi\left(^3D_2,\,FM_F\right)\right\rangle}{E\left(^3D_2\right) \;-\; E\left(^3P_1\right)} \tag{11}$$

if the summation over the intermediate states is restricted to the nearby $^3P_1$ level. This assumption is justified by the size of the energy denominator which is 500 times smaller than the second smallest. Moreover, the electron nucleus interaction in equation (5) is scalar, therefore only one of the hyperfine states may occur.

When the multiconfiguration expansion from Eq. (1) is employed for the electronic part of the (total) wave functions, the reduced matrix elements of general tensor operator $\hat{T}^k_q$ can be decomposed into (reduced) matrix

elements between configuration state functions

$$\left[\Psi\left(\gamma PJ\right)\|\hat{T}^k\|\Psi\left(\alpha(-P)J_i\right)\right] = \sum_{r,s} c_r c_s \left[\Phi\left(\gamma_r PJ\right)\|\hat{T}^k\|\Phi\left(\gamma_s(-P)J_i\right)\right] \quad (12)$$

and those, in turn, into a sum of single-particle matrix elements

$$\left[\Phi\left(\gamma_r PJ\right)\|\hat{T}^k\|\Phi\left(\gamma_s(-P)J_i\right)\right] = \sum_{a,b} d^k_{ab}(rs)\left[n_a\kappa_a\|\hat{t}^k\|n_b\kappa_b\right]. \quad (13)$$

In the latter expansion, the $d^k_{ab}(rs)$ are known as 'angular coefficients' that arise from using Racah's algebra in the decomposition of the many-electron matrix elements [27, 36]. The single-particle reduced matrix elements in the expansion (13) can be factorized into reduced angular matrix elements and radial integrals which, for the Schiff moment interaction, read

$$\left[n_a\kappa_a\|\hat{\nabla}^1\,\rho\left(r\right)\|n_b\kappa_b\right] = \left[\kappa_a\|C^1\|\kappa_b\right]\int_0^\infty \left(P_aP_b + Q_aQ_b\right)\frac{d\rho}{dr}\,dr\,, \quad (14)$$

while for the electric-dipole moment operator ($k = 1$) it is

$$\left[n_a\kappa_a\|\hat{d}^1\|n_b\kappa_b\right] = -\left[\kappa_a\|C^1\|\kappa_b\right]\int_0^\infty \left(P_aP_b + Q_aQ_b\right)\,r\,dr. \quad (15)$$

For the calculations of the matrix elements we extended the GRASP [28] and *mdfgme* [37] relativistic atomic structure packages. The extension, presented in this work, includes programs for both Schiff moment interaction and electric-dipole moment matrix elements. Experimental energy differences were used in the calculations of all expectation values. The energy values for the two levels of interest ($E_{7s6d\ ^3D_2} = 13993.97cm^{-1}$ and $E_{7s7p\ ^3P_1} = 13999.38cm^{-1}$) were taken from the tables of Moore [38]. The nuclear spin and magnetic moment data were taken from the tables of Raghavan [39].

D. Handling non-orthogonalities

The electronic wave functions were optimised separately for the two levels of interest. All expectation values were evaluated with the biorthogonal technique developed by Malmquist [40]. For two atomic state functions

$$\Psi(\gamma PJ) = \sum_r c_r\Phi(\gamma_r PJ) \quad (16)$$

and

$$\Psi(\alpha(-P)J_i) = \sum_s c_s\Phi(\gamma_s(-P)J_i) \quad (17)$$

the reduction of a general matrix element

$$\left[\Psi\left(\gamma PJ\right)\|\hat{T}^k\|\Psi\left(\alpha(-P)J_i\right)\right] \quad (18)$$

into a sum of *radial integral* × *angular coefficient* terms is based on tensor algebra techniques. In the decomposition (13), it is usually assumed that the (many-electron) configuration states on both sides of the matrix element are built from a common set of spin-orbitals. This is a very severe restriction since a high-quality wave function demands orbitals optimized for the specific electronic state. Instead of the standard decomposition (13) based on tensor algebra techniques, Malmquist has shown [40] that for very general expansions, where the two atomic states are described by different orbital sets, it is possible to transform the wave function representations of the two states in such a way that standard techniques can be used for the reduction of the matrix elements in the new representation. This procedure has been implemented in the modules that compute Schiff moments and it can be summarized as follows

1. Perform MCDHF or CI calculations for the two states where the orbital sets of the two wave functions are not required to be identical.
2. Change the wave function representations by transforming the two orbital sets to a biorthogonal basis. This is followed by a counter-transformation of the expansion coefficients c_r and c_s so as to leave the resultant wave functions invariant.
3. Calculate the matrix elements with the transformed wave functions for which now standard techniques can be used [27].

The transformation of wave functions is very fast, since it relies only on angular coefficients for a one-electron operator of rank zero which appears in the evaluation of the kinetic energy term in the MCDHF or CI step. The details of the transformations are discussed in [41].

III. METHOD OF CALCULATION

To generate the atomic states of interest, the method described as systematic expansion of configuration set [30, 31] has been employed, in which symmetry-adapted CSF of a given parity and total angular momentum are generated by substitutions from reference configurations to an active set of orbitals. The active set should hereby comprise (at least) all valence shells, several 'near-valence' core shells, as well as certain number of virtual shells. The active set and multiconfiguration expansions are then systematically increased until the expectation value (of interest) is converged. In practice, we divided

the computations into three phases to generate (i) the spectroscopic orbitals, (ii) the virtual orbitals, and (iii) to perform large configuration interaction calculations, once the set of orbitals is fixed.

A. Orbital set

In the first phase of the computations, all spectroscopic orbitals required to form a reference wave function were obtained with a minimal configuration expansion, with full relaxation. These orbitals were determined from a symmetry-adapted Dirac-Fock calculation with only those configurations which arise in *j*-*j* coupling for a particular state of interest. The spectroscopic orbitals were kept frozen in all later steps.

In the second phase the virtual orbitals were generated in five consecutive steps. At each step the virtual set has been extended by one layer of virtual orbitals. A layer is defined as a set of virtual orbitals with different angular symmetries. In the present paper five layers of virtual orbitals were generated, each layer comprising orbitals with symmetries *s,p,d,f,g,* and *h*. At each step the configuration expansions were limited to single and double substitutions from valence shells to all new orbitals as well as to all (virtual) orbitals of the previously generated layers. These substitutions were augmented by a small subset of dominant single and double substitutions from core and valence shells, with the further restriction that at most one electron may be promoted from the core shells (i.e. in a double substitution at least one electron is promoted from a valence shell). All configurations from earlier steps were retained, with all previously generated orbitals fixed, and all new orbitals made orthogonal to all others of the same symmetry. The initial shapes of radial orbitals were obtained by means of a Thomas-Fermi potential, and then driven to convergence with the self-consistency threshold set to 10^{-10} for spectroscopic orbitals and 10^{-8} for virtual orbitals, respectively. All radial orbitals were separately optimized for each atomic state. The Optimal Level form of the variational expression [32] was applied in all variational calculations.

B. Configuration-interaction calculations

In the third phase of the computations, the configuration-interaction calculations (i.e. without changing the radial shapes of the one-electron spin-orbitals) were performed, with multiconfiguration expansions tailored in such a way, as to capture the dominant electron correlation contributions to the expectation values. All single and double substitutions were allowed from several core shells and from both valence subshells (i.e. $7s7p$, or $7s6d$, depending on the state) to all virtual shells, with the same restriction as above, i.e. that at most one electron may be promoted from core shells. The virtual set was systematically increased from one to five layers. In a similar manner, several core subshells were systematically opened for electron substitutions — from the outermost $6p$ up to the $5s5p5d6s6p$ subshells.

The convergence of the calculations can be observed by monitoring the dependence of the matrix elements on the size of the virtual set as well as on the number of core subshells that are opened for electron substitutions. The effects of substitutions from $4s4p4d4f$ and still deeper shells were estimated in our previous papers and turned out to be below 1 percent in the case of hyperfine structures [42, 43] and a fraction of a percent in the case of transition rates [44, 45].

TABLE I: The values of the reduced matrix element of the Schiff operator $4\sqrt{3}\,\pi\,\left[{}^3P_1\left\|\hat{\nabla}^1\,\rho\,(r)\right\|{}^3D_2\right]$ from Eq. (10) [a.u.]. Electron substitutions *from* different sets of spectroscopic orbitals: $6p[7s6d|7s7p]$ (second column), $6sp[7s6d|7s7p]$ (third column), ... , $5spd6sp[7s6d|7s7p]$ (sixth column). Electron substitutions *to* different sets of virtual orbitals: (1v) one layer of virtual orbitals, (2v) two layers of virtual orbitals, ... , (5v) five layers of virtual orbitals. 'DF' = uncorrelated Dirac-Fock value.

DF	674				
virtual	shells opened for substitutions				
set	6p	6sp	5d6sp	5pd6sp	5spd6sp
1v	1931	1892	1862	1749	1647
2v	4597	7544	7553	7598	7754
3v	5141	8073	8112	8125	8327
4v	4760	7936	7947	7889	8117
5v	4642	7834	7818	7743	8217

IV. RESULTS

Table I shows the values of the reduced matrix element of the Schiff operators $4\sqrt{3}\;\pi\;\left[{}^3P_1\left\|\hat{\nabla}^1\,\rho\,(r)\right\|{}^3D_2\right]$ from Eq. (10). The expectation values were calculated for the multiconfiguration expansions obtained from all possible combinations of virtual sets, and from opening sequentially the core subshells, as described in section III B.

Table II presents the values of the reduced matrix element of the EDM operator $\sqrt{3}\,\left[{}^3P_1\,\|-er\|\,{}^3D_2\right]$ from Eq. (9). As in Table I, the EDM matrix elements were calculated for the multiconfiguration expansions resulting from all possible combinations of virtual sets and from opening up the core subshells, cf. section III B.

The data from Tables I and II are collected also in Figure 2, where they are presented as functions of the size NCF (see Eq. 1) of the multiconfiguration expansion. Figure 2(a) shows the reduced matrix element of the Schiff operator, while Figure 2(b) shows the value of reduced matrix element of EDM operator. The resultant EDM, induced by the nuclear Schiff moment in the ${}^3D_2$ state of the isotope Ra-223 is presented in Table III.

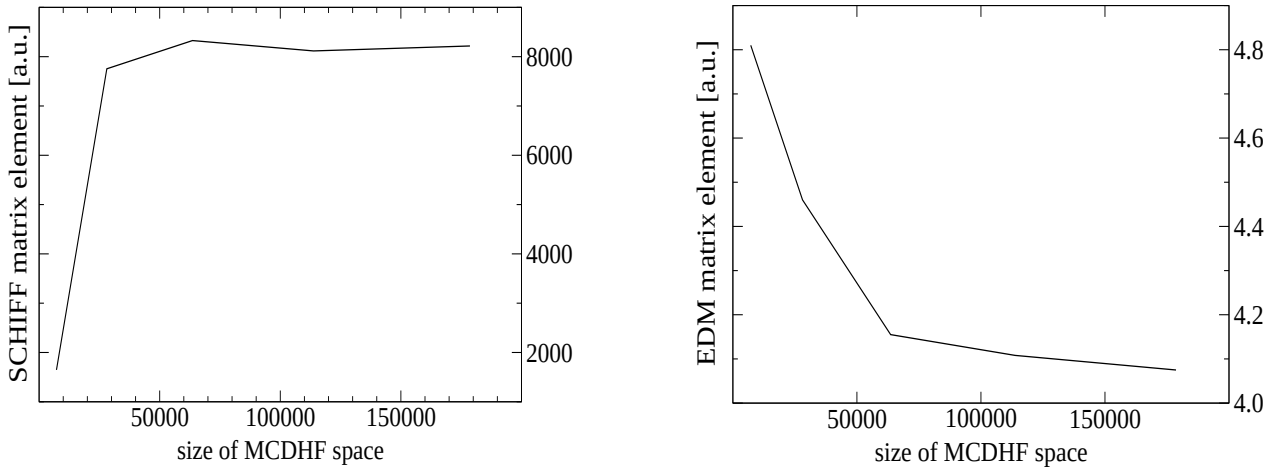

(a) Schiff (b) EDM

FIG. 2: The values of the reduced matrix elements of the (a) Schiff and (b) EDM operators as functions of the size of the multiconfiguration expansion

TABLE II: The values of the reduced matrix element of the EDM operator $\sqrt{3}\ \left[{}^3P_1\,\|-er\|\,{}^3D_2\right]$ from Eq. (9) [a.u.]. The notations are the same as in Table I.

DF	5.849				
virtual	shells opened for substitutions				
set	6p	6sp	5d6sp	5pd6sp	5spd6sp
1v	4.818	4.811	4.810	4.810	4.810
2v	4.514	4.467	4.460	4.460	4.460
3v	4.270	4.192	4.157	4.155	4.155
4v	4.251	4.168	4.114	4.109	4.108
5v	4.240	4.153	4.083	4.076	4.075

A. Electron correlation effects

The calculations appear to be converged within the multiconfiguration approximation employed in the present paper. A comparison of the 'DF' value with the final result in Table III shows, that correlation effects are dominant in these calculations. An inspection of Tables I and II reveals that the Schiff moment matrix element is mainly responsible for the correlation correction to the atomic EDM. Overall, the correlated Schiff value is more than an order of magnitude larger than the uncorrelated one. On the other hand, the correlated value of the EDM matrix element is about 30% smaller than the uncorrelated one. Together, they result in the atomic EDM, which is 8.5 times larger than the uncorrelated value. There are several factors, which have to be taken into consideration in these calculations in order to capture the bulk of the electron correlation effects:

1. Schiff interaction is localised inside nucleus (see Eq. 14), therefore only the (one-electron) matrix elements $\left[s_{1/2}\|\hat{\nabla}^1\,\rho\,(r)\,\|p_{1/2}\right]$ and $\left[s_{1/2}\|\hat{\nabla}^1\,\rho\,(r)\,\|p_{3/2}\right]$ contribute appreciably in Eq. (13) (see also Table II in ref. [17]). All other spin-orbitals may contribute through the indirect electron correlation effects [46].
2. Only the inner regions of the spin-orbitals contribute to the Schiff moment matrix elements. Therefore it is essential to accurately represent core polarisation in the atomic wave functions.
3. For the electric dipole interaction, the outer parts of the spin-orbitals are important. Therefore the valence correlation effects have to be accounted for. The Babushkin and Coulomb gauge values differ by 5 orders of magnitude in the calculation of the very weak ${}^3P_1 - {}^3D_2$ transition [45]. This results from the fact, that the transition energy is very small. Transition energy is difficult to reproduce accurately in variational calculations, when the wave functions for the two levels are generated separately and when their one-electron orbitals are optimised independently. It is necessary to obtain a balanced description of both states [47], which can only be achieved if all two-body (double substitu-

TABLE III: The atomic EDM D_A $[10^9 S/I]$ of the $|F, M_F\rangle = |3/2, 3/2\rangle$ hyperfine state of the ${}^3D_2$ level, induced by the nuclear Schiff moment in the isotope ${}^{223}_{88}$Ra ($I = \frac{3}{2}$) [a.u.]. The notations are the same as in Table I.

DF	0.0512				
virtual	shells opened for substitutions				
set	6p	6sp	5d6sp	5pd6sp	5spd6sp
1v	0.1812	0.1181	0.1163	0.1092	0.1028
2v	0.2694	0.4378	0.4374	0.4399	0.4489
3v	0.2850	0.4393	0.4378	0.4383	0.4492
4v	0.2627	0.4293	0.4244	0.4208	0.4329
5v	0.2555	0.4224	0.4144	0.4097	0.4346

tions) and possibly also three- and four-body (triple and quadruple substitutions) correlation effects are fully taken into account. In general, the two gauges exhibit different energy dependence: the Coulomb gauge is strongly energy dependent, therefore the Babushkin gauge value is usually adopted in unsaturated calculations, since it is less dependent on calculated transition energy value. The calculations of energy level differences require well balanced orbital sets and typically demand highly extensive multiconfiguration expansions. The results are usually in better agreement with experiment if a common set of orbitals is used for both states.

4. On the other hand, the wave functions for the two levels have to be generated separately, if the effects of non-orthogonality are to be taken into account correctly. Non-orthogonality between the spin-orbitals is essential in the evaluation of non-diagonal matrix elements (see Ref. [45].

B. Breit and QED corrections

The calculations descibed in the previous sections as well as the data in Tables I, II, and III were obtained with only the Coulomb interaction included in the differential equations which are iteratively solved during the self-consistent field process (SCF). The effects of magnetic and retardation corrections can be evaluated by introducing the full Breit operator in the self-consistent field process. Such modified differential equations lead to change of the final wavefunction shape, which in turn modifies the matrix elements evaluated in the calculation of the Schiff moment. Quantum electrodynamics (QED) correction is dominated by two contributions. The self-energy (SE) part cannot be easily evaluated. Its contribution to the Cs parity violation amplitude has been calculated in Ref. [48] and turned out to be of the order of -0.7 %. On the other hand, the vacuum polarization can be easily calculated by introducing the Uelhing potential into the SCF, as was done, for example, in calculations of Li-like ions hyperfine matrix elements [49] or in Cs parity-violation amplitude [50]. In the latter case, it leads to a 0.4 % increase of the amplitude. If both are evaluated, the SE and VP contributions partly compensate. We have used the *mdfgme* code [37] in its 2008 version, which now includes a Schiff moment option, to evaluate the effect of the Breit interaction and vacuum polarization on the Schiff moment. The results are presented in Table IV. The inclusion of the Breit interaction in the SCF reduced the value of the Schiff moment by a factor of 1.7 %, while the vacuum polarization increased it by roughly 0.6 %. The total correction is a reduction of the order of 1.1 %. From Ref. [48] one should expect a partial, mutual compensation of the VP and SE contributions. The total correction would then be dominated by the Breit contribution.

The results presented in Table IV were obtained in single configuration approximation, i.e., without electron correlation effects. Our experience indicates, that a fully correlated calculation, i.e., with the multiconfiguration expansion (1) described in section III B, and with the self-consistent Breit interaction would lead to a larger (absolute value of) total correction. However, the increase of the number of extra integrals involved (roughly by 2 orders of magnitude) and substantial convergence difficulties render such a calculation virtually impossible with today's computers.

	Schiff	Stark	EDM	correction
DF	674	5.849	0.0512	
Breit SCF	664	5.835	0.0503	−1.7 %
Breit SCF + VP SCF	668	5.837	0.0507	−1.1 %

TABLE IV: Effect of the Breit and vacuum polarization on the reduced matrix element of the Schiff operator (Schiff), reduced matrix element of the EDM operator (Stark), and the atomic EDM (D_A $[10^9 S/I]$) of the $|F, M_F\rangle = |3/2, 3/2\rangle$ hyperfine state of the $^3D_2$ level, induced by the nuclear Schiff moment in the isotope $^{223}_{88}$Ra ($I = \frac{3}{2}$) [a.u.]. VP — vacuum polarization. DF — Coulomb interaction only.

The final correction from Table IV (i.e., the reduction by a factor of 0.989 %) has been carried over to the final summary of our results, which is presented in Table V.

C. Accuracy

Although we have full control of the core polarisation effects, the overall accuracy of these results depends primarily on the electron-correlation effects which were not included in the calculations, i.e. unrestricted double substitutions and triple substitutions. These unrestricted substitutions had to be omitted due to software and hardware limitations. A similar approximation, based on single and restricted double substitutions, was employed also in our previous papers on radium [42, 43, 44, 45]. The accuracy of the present calculations can be indirectly inferred from a comparison of the previously calculated transition rates and hyperfine constants with experiment. Reference [43] showed hyperfine constants calculated in an approach similar to that employed in the present paper. As discussed there, the overall accuracy of the calculated magnetic dipole constants was 6 %, while for the electric quadrupole constants the estimated accuracy was 3 %. The interaction responsible for the hyperfine shifts takes place in the vicinity of the nucleus. The bulk of the hyperfine integral/matrix elements come from the first oscillation of the one-electron wave function [51, 52]. Therefore, the calculated hyperfine constants depend heavily on the inner regions of the one-electron wave functions. The interaction of the electronic cloud with the nuclear Schiff moment also takes place in the vicinity of the nucleus. In fact, the bulk of the Schiff integral/matrix element comes from the nuclear skin (see

Eq. 14). Therefore we might expect that the accuracy of the calculated Schiff moment matrix elements is comparable to the accuracy of the calculated hyperfine constants. In conclusion, we might expect the accuracy of the calculated Schiff moment matrix elements of the order of 10 % or better.

The electric-dipole moment matrix element (see Eq. 15) has similar radial dependence as the electric-dipole transition elements, therefore their accuracy might also be expected to be of the same order. The calculated rate for the strong transition $^1P_1 - {}^1S_0$ showed excellent agreement between the values calculated in Babushkin and Coulomb gauges [44], which is an indication (but not a proof) of convergence. The accuracy of the calculated rate for the $^3P_1 - {}^1S_0$ transition was also reasonably good [45]. Although there was a 20 % difference between the values calculated in the two gauges, the Babushkin gauge value fell within the experimental limit [53]. The gauge difference was somewhat larger (35 %) for the calculated rate for the $^3D_2 - {}^1S_0$ electric quadrupole transition [44] which is the only significant decay channel of the metastable state $^3D_2$. However, the calculated rates of other weak transitions were less accurate. In particular, the calculated rate for the $^3P_1 - {}^3D_2$ transition showed very large gauge dependence, which seems to indicate that the core-core correlation effects (which were omitted in present calculations) are important (see e.g. [54]). These correlation contributions are currently beyond the capacity of the computer resources available to us. We were unable to include, or even to estimate the contributions of the omitted electron correlation effects, i.e., the unrestricted double substitutions and triple substitutions, to the atomic EDM. Such calculation would require a multiprocessor cluster in excess of a hundred processors [55]. In order to estimate the uncertainty of the electric dipole moment calculation, we had to resort to an upper limit resulting from the hierarchy of electron-electron interactions. Table II demonstrates the saturation of the core-valence correlation correction, which is the dominant electron correlation effect beyond the Dirac-Fock approximation. Therefore we might expect that the entire (core-valence) electron correlation contribution would be a rather conservative estimate of the uncertainty of the electric dipole moment calculations. In conclusion, we may assume the accuracy of the calculated electric dipole moment matrix elements of the order of 30 %.

Another contribution that affects the overall accuracy of the results arises from the nuclear-density dependence of radial matrix elements in Eq. (14), i.e. from the distribution of the nuclear charge, as discussed in section II B. However, the error of the calculated value of atomic EDM is dominated by the electric dipole moment calculation. Therefore we assumed 30 % accuracy of the final calculated value of the Schiff moment enhancement factor, as shown in Table V.

A more stringent accuracy assessment for the present calculations would require more experimental data to compare with. Hereby, we would like to encourage the experimenters to provide them. In particular, hyperfine constants for other levels, as well as lifetime and transition rate measurements for weak transitions would be very valuable.

TABLE V: The atomic EDM induced by the nuclear Schiff moment in the $^3D_2$ electronic state for three isotopes of radium: $^{213}_{88}$Ra ($I = \frac{1}{2}, F = \frac{3}{2}$), $^{223}_{88}$Ra ($I = \frac{3}{2}, F = \frac{3}{2}$), and $^{225}_{88}$Ra ($I = \frac{1}{2}, F = \frac{3}{2}$), respectively. Results are shown as functions of the size of the virtual orbital set, including electron substitutions from the spectroscopic $5spd6sp[7s6d|7s7p]$ orbitals to: (1v) one layer of virtual orbitals, (2v) two layers of virtual orbitals, ... , (5v) five layers of virtual orbitals. 'DF' = uncorrelated Dirac-Fock value. Our values include the 'Breit SCF + VP SCF' correction from Table IV. The RHF+CI results in the last line are quoted from Ref. [17].

	EDM $[10^9 S/I]$ [a.u.]		
layer	$^{213}_{88}$Ra	$^{223}_{88}$Ra	$^{225}_{88}$Ra
DF	0.0159	0.0507	0.0158
1v	0.0320	0.1017	0.0318
2v	0.1393	0.4441	0.1387
3v	0.1394	0.4444	0.1388
4v	0.1344	0.4283	0.1338
5v	0.1349	0.4300	0.1343
final	0.13(4)	0.43(14)	0.13(4)
RHF+CI	0.094	0.30	0.094

The results presented in the second and in the last column of Table V illustrate the isotope-dependence of the atomic EDM. The two isotopes in question, $^{213}_{88}$Ra and $^{225}_{88}$Ra, have the same nuclear spin ($I = 1/2$), but they have slightly different nuclear shapes (see Eq. (3) and the subsequent discussion in section II B). The abovementioned isotope-dependence, of the order of 0.4 %, arises primarily through the derivative $d\rho/dr$ in Eq. (14). The isotope-dependence of the atomic wave functions (1) has been neglected in the present calculations.

V. CONCLUSIONS

Radium is well suited for EDM experiments because of its large nuclear charge Z and the two low-lying levels $^3P_1$ and $^3D_2$ of opposite parity, which are separated in energy by only 5 cm^{-1} $\approx 2 \times 10^{-5}$ a.u. The $^3D_2$ level is metastable with a very long lifetime of the order of 4 seconds [45] and therefore suitable for laser-ion traps. For radium, moreover, there are several isotopes with mass ranging from 209 up to 229, of which $^{213}_{88}$Ra and $^{225}_{88}$Ra have nuclear spin $I = 1/2$. For EDM experiments the $I = 1/2$ isotopes are preferable since these isotopes cannot be disturbed by higher order electromagnetic moments.

The paper presents systematic computations of the static EDM of atomic radium in the $^3D_2$ level, induced

by the nuclear Schiff moment. Table V shows the atomic EDM induced by the nuclear Schiff moment in the $^3D_2$ electronic state for three isotopes of radium:

$^{213}_{88}$Ra ($I = \frac{1}{2}, F = \frac{3}{2}, \mu = 0.6133$),
$^{223}_{88}$Ra ($I = \frac{3}{2}, F = \frac{3}{2}, \mu = 0.2705$), and
$^{225}_{88}$Ra ($I = \frac{1}{2}, F = \frac{3}{2}, \mu = -0.7338$).

The wave functions for the two levels, $^3P_1$ and $^3D_2$, were generated separately, in order to correctly reproduce the effects of non-orthogonality between one-electron spinorbitals. We demonstrate that core-valence electron correlation, which is the dominant electron correlation effect beyond the Dirac-Fock approximation, contributes almost 90% of the total EDM value. Our final value is about 30% larger than the RHF+CI result from Ref. [17]. The difference can be atributed to different methods employed to account for core-valence electron correlation effects. Neither of these two calculations included the core-core correlation effects, which we believe to be the dominant source of uncertainty in our calculated value of the Schiff moment enhancement factor.

Acknowledgements

This work was supported by the Polish Ministry of Science and Higher Education (MNiSW) in the framework of the scientific grant No. 1 P03B 110 30 awarded for the years 2006-2009. SF acknowledges the support by the DFG under the project No. FR 1251/13. EG acknowledges the Student Research Fellowship Award from the Lithuanian Science Council. PJ acknowledges the support from the Swedish Research Council (Vetenskapsrådet). PI acknowledges the support of the Helmholtz Alliance Program of the Helmholtz Association, contract HA-216 "Extremes of Density and Temperature: Cosmic Matter in the Laboratory". Laboratoire Kastler Brossel is "Unité Mixte de Recherche du CNRS, de l'ENS et de l'UPMC n° 8552". We would like to thank Klaus Jungmann, Jeffrey Guest, William Trimble and Jean-Paul Desclaux for helpful discussions.

[1] A.-M. Mårtensson-Pendrill, in *Methods in Computational Chemistry*, edited by S. Wilson (Plenum Press, New York, 1992), vol. 5, pp. 99–156.
[2] I. B. Khriplovich and S. K. Lamoreaux, *CP Violation Without Strangeness* (Springer, Berlin, 1997).
[3] J. S. M. Ginges and V. V. Flambaum, Phys. Rep. **397**, 63 (2004).
[4] T. Legero, T. Wilk, M. Hennrich, G. Rempe, and A. Kuhn, Phys. Rev. Lett. **93**, 070503 (2004).
[5] S. Kuhr, W. Alt, D. Schrader, I. Dotsenko, Y. Miroshnychenko, A. Rauschenbeutel, and D. Meschede, Phys. Rev. A **72**, 023406 (2005).
[6] J. Beugnon, M. P. A. Jones, J. Dingjan, B. Darquié, G. Messin, A. Browaeys, and P. Grangier, Nature **440**, 779 (2006).
[7] J. R. Guest, N. D. Scielzo, I. Ahmad, K. Bailey, J. P. Greene, R. J. Holt, Z.-T. Lu, T. P. O'Connor, and D. H. Potterveld, Phys. Rev. Lett. **98**, 093001 (2007).
[8] U. Dammalapati, S. De, K. Jungmann, and L. Willmann, arXiv:0708.0332v1 [physics.atom-ph].
[9] V. A. Dzuba, V. V. Flambaum, J. S. M. Ginges, and M. G. Kozlov, Phys. Rev. A **66**, 012111 (2002).
[10] N. D. Scielzo, J. R. Guest, E. C. Schulte, I. Ahmad, K. Bailey, D. L. Bowers, R. J. Holt, Z.-T. Lu, T. P. O'Connor, and D. H. Potterveld, Phys. Rev. A **73**, 010501(R) (2006).
[11] URL www-mep.phy.anl.gov/atta/research/radiumedm.html.
[12] K. Jungmann, Acta Phys. Pol. B **33**, 2049 (2002).
[13] Klaus Jungmann, private communication.
[14] URL www.kvi.nl/∼trimp/web/html/trimp.html.
[15] J. Engel, M. Bender, J. Dobaczewski, J. H. de Jesus, and P. Olbratowski, Phys. Rev. C **68**, 025501 (2003).
[16] J. Dobaczewski and J. Engel, Phys. Rev. Lett. **94**, 232502 (2005).
[17] V. A. Dzuba, V. V. Flambaum, and J. S. M. Ginges, Phys. Rev. A **61**, 062509 (2000).
[18] V. V. Flambaum, Phys. Rev. A **60**, R2611 (1999).
[19] Jeffrey Guest, private communication.
[20] William Trimble, private communication.
[21] G. Gaigalas, E. Gaidamauskas, and P. Jönsson, Journal of Physics. Conference series **130**, 012008 (2008).
[22] I. Lindgren and J. Morrison, *Atomic Many-Body Theory* (Springer, Berlin, 1986).
[23] V. A. Dzuba, Phys. Rev. A **71**, 032512 (2005).
[24] V. A. Dzuba and V. V. Flambaum, Phys. Rev. A **75**, 052504 (2007).
[25] W. R. Johnson, *Atomic Structure Theory: Lectures on Atomic Physics* (Springer, Berlin, 2007).
[26] I. P.Grant, *Relativistic Atomic Structure Calculations*, vol. 2 of *Methods in Computational Chemistry* (Plenum Press, New York, 1988), edited by S. Wilson.
[27] I. P. Grant, *Relativistic Quantum Theory of Atoms and Molecules: Theory and Computation* (Springer, New York, 2007).
[28] P. Jönsson, X. He, C. Froese Fischer, and I. P. Grant, Comput. Phys. Commun. **177**, 597 (2007).
[29] I. P. Grant, Comput. Phys. Commun. **84**, 59 (1994).
[30] J. Bieroń, P. Jönsson, and C. Froese Fischer, Phys. Rev. A **53**, 2181 (1996).
[31] J. Bieroń, P. Jönsson, and C. Froese Fischer, Phys. Rev. A **60**, 3547 (1999).
[32] K. G. Dyall, I. P. Grant, C. T. Johnson, F. A. Parpia, and E. P. Plummer, Comput. Phys. Commun. **55**, 425 (1989).
[33] W. R. Johnson and G. Soff, At. Data Nucl. Data Tables **33**, 405 (1985).
[34] URL http://dirac.chem.sdu.dk/doc/FiniteNuclei/FiniteNuclei.shtml.
[35] This approach is well justified since each *non-diagonal* term in Eq. (4) leads to an additional summation in the expansion (6) $\sum_j c_j \Psi(..PJ'..)$, with coefficients of the order $10^{-5}...10^{-10}$, owing to weakness of the hyperfine interaction. These coefficients are to be compared with

$a \approx 1$ in Eq. (6), and, hence, they strongly suppress the non-diagonal terms of the hyperfine structure.

[36] G. Gaigalas, S. Fritzsche, and I. P. Grant, Comput. Phys. Commun. **139**, 263 (2001).

[37] P. Indelicato and J.-P. Desclaux, *MCDFGME, a MultiConfiguration Dirac-Fock and General Matrix Elements program (release 2005)*, URL `http://dirac.spectro.jussieu.fr/mcdf`.

[38] C. E. Moore, *Atomic Energy Levels,* NSRDS-NBS No 35, (Washington DC: US Govt. Printing Office) (1971).

[39] P. Raghavan, At. Data Nucl. Data Tables **42**, 189 (1989).

[40] P. Å. Malmqvist, Int. J. Quantum Chem. **30**, 479 (1986).

[41] J. Olsen, M. R. Godefroid, P. Jönsson, P. Å. Malmqvist, and C. Froese Fischer, Phys. Rev. E **52**, 4499 (1995).

[42] J. Bieroń and P. Pyykkö, Phys. Rev. A **71**, 032502 (2005).

[43] J. Bieroń, J. Phys. B: At. Mol. Opt. Phys. **38**, 2221 (2005).

[44] J. Bieroń, C. Froese Fischer, S. Fritzsche, and K. Pachucki, J. Phys. B: At. Mol. Opt. Phys. **37**, L305 (2004).

[45] J. Bieroń, P. Indelicato, and P. Jönsson, Eur. Phys. J. Special Topics **144**, 75 (2007).

[46] J. Bieroń, C. F. Fischer, P. Jönsson, and P. Pyykkö, J. Phys. B: At. Mol. Opt. Phys. **41**, 115002 (2008).

[47] C. Froese Fischer, Phys. Scr. **T83**, 49 (1999).

[48] V. M. Shabaev, K. Pachucki, I. I. Tupitsyn, and V. A. Yerokhin, Phys. Rev. Lett. **94**, 213002 (2005).

[49] S. Boucard and P. Indelicato, Eur. Phys. J. D **8**, 59 (2000).

[50] W. R. Johnson, I. Bednyakov, and G. Soff, Phys. Rev. Lett. **87**, 233001 (2001).

[51] P. Pyykkö, J. Magn. Res. **8**, 15 (1972).

[52] P. Pyykkö, E. Pajanne, and M. Inokuti, Int. J. Quantum Chem. **7**, 785 (1973).

[53] N. D. Scielzo, J. R. Guest, E. C. Schulte, I. Ahmad, K. Bailey, D. L. Bowers, R. J. Holt, Z.-T. Lu, T. P. O'Connor, and D. H. Potterveld, Phys. Rev. A **73**, 010501(R) (2006).

[54] P. Jönsson, A. Ynnerman, C. Froese Fischer, M. R. Godefroid, and J. Olsen, Phys. Rev. A **53**, 4021 (1996).

[55] J. Bieroń, C. Froese Fischer, P. Indelicato, P. Jönsson, and P. Pyykkö, arXiv:0902.4307v1 [physics.atom-ph].